# Mitophagy of polarized sperm-derived mitochondria after fertilization

Karinna Rubio-Peña, Sara Al Rawi, Fanny Husson, France Lam, Jorge Merlet, Vincent Galy

iScience

CellPress
OPEN ACCESS

Article

# Mitophagy of polarized sperm-derived mitochondria after fertilization

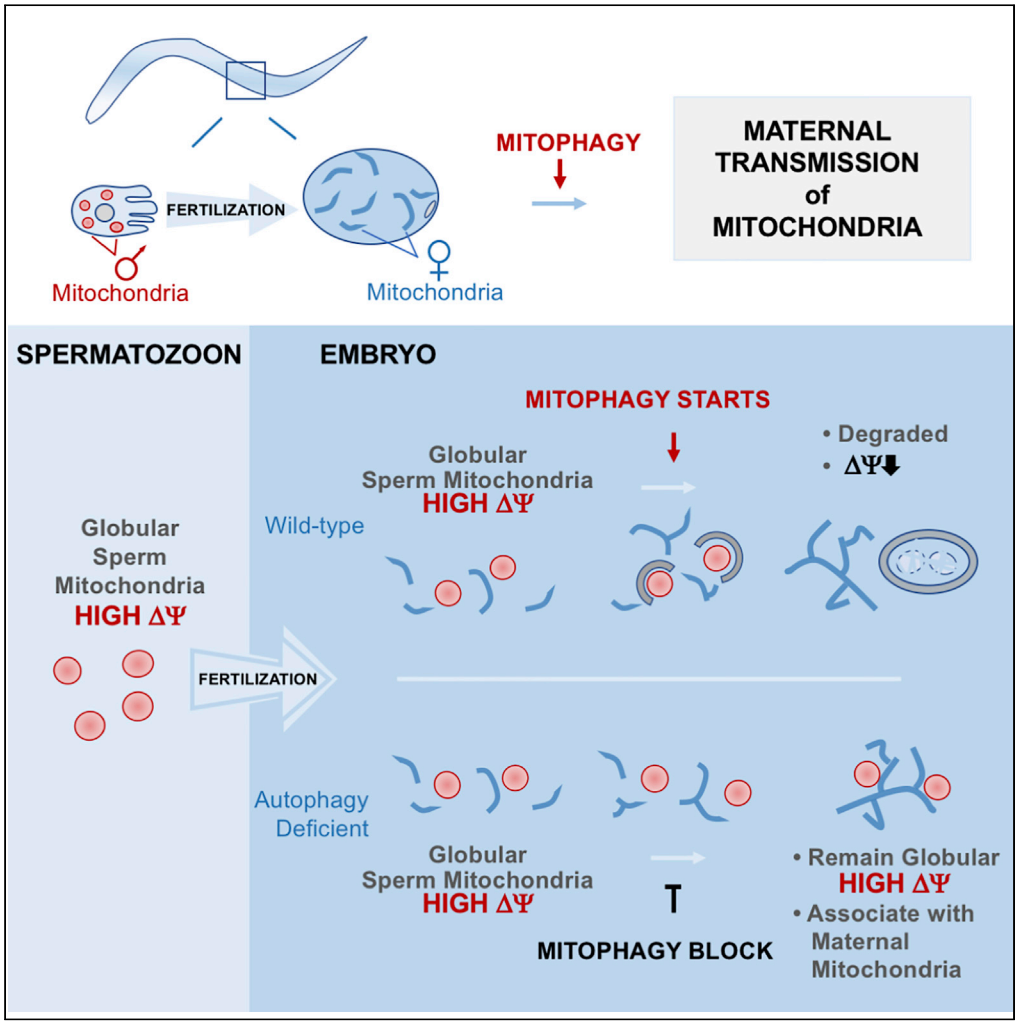


Karinna Rubio-Peña, Sara Al Rawi, Fanny Husson, France Lam, Jorge Merlet, Vincent Galy

vincent.galy@sorbonne-universite.fr

## HIGHLIGHTS

Oocyte-derived mitochondria become tubular only during the first zygotic division

Sperm mitochondria can not fuse but associate with the oocyte-derived mitochondria

Sperm mitochondria are still polarized when engulfed for autophagy degradation

Rubio-Peña et al., iScience 24, 102029
January 22, 2021 
https://doi.org/10.1016/j.isci.2020.102029

iScience

CellPress
OPEN ACCESS

Article

# Mitophagy of polarized sperm-derived mitochondria after fertilization

Karinna Rubio-Peña,[1] Sara Al Rawi,[1] Fanny Husson,[1] France Lam,[2] Jorge Merlet,[1] and Vincent Galy[1,3,*]

## SUMMARY

**Loss of membrane potential of sperm mitochondria has been regarded as the first step preceding mitophagy degradation after their entry into the *C. elegans* oocyte at fertilization. This is in line with the classical view of mitophagy of defective or abnormal mitochondria and could serve as a recognition signal for their specific and quick autophagy degradation. Here, using TMRE (tetramethylrhodamine ethyl ester) and live imaging we show that this is not the case. Instead, sperm inherited mitochondria show a stable labeling with TMRE before and at the time of autophagosomes formation. Interestingly, this labeling remains in late-stage-embryos of autophagy-defective-mutants suggesting that the loss of membrane potential occurs upon the entry of the mitochondria into the autophagy pathway. These stabilized and still polarized sperm mitochondria remain distinct but associated with the maternal-derived mitochondrial network suggesting a mechanism that prevents their fusion and represents an efficient additional protective system against fertilization-induced heteroplasmy.**

## INTRODUCTION

For years, the maternal inheritance of the mitochondrial genome was considered as the result of a large dilution of paternal mitochondria contribution with respect to maternal load (Song et al., 2016b; Sutovsky and Song, 2018). Now we know that it relies on a combination of various active mechanisms that prevent the transmission of sperm mitochondrial genome. Among these, the degradation of sperm mitochondria and their genome after their entry into the oocyte has been observed in various vertebrate and invertebrate species (DeLuca and O'Farrell, 2012; Politi et al., 2014; Al Rawi et al., 2011; Sato and Sato, 2011; Song et al., 2016a). In *C. elegans*, the degradation of the sperm-inherited mitochondria by the autophagy machinery starts around 20 min after embryonic fertilization and completes within 2 hr, before the embryo reaches the 16-cell stage (Al Rawi et al., 2011; Sato and Sato, 2011). The recruitment of the LC3/ATG8 homologs LGG-1 and LGG-2 membrane associated ubiquitin like proteins around sperm mitochondria and the golgi-derived nematode-specific membranous organelles starts at the end of the female's first meiotic division, 15-20 minutes after fertilization. The autophagosome formation occurs around 50 individualized globular sperm mitochondria ensuring maternal mitochondrial genome inheritance. Recently, the observation of a rapid loss of membrane potential, which was based on the loss of TMRE (tetramethylrhodamine ethyl ester), a cationic mitochondrial fluorescent marker from pre-loaded sperm-mitochondria, was described as the first event occurring between sperm entry and autophagosome formation (Sato et al., 2018; Wang et al., 2016; Zhou et al., 2016). Interestingly, this premature loss of mitochondria membrane potential in sperm-derived mitochondria was observed even in mutants stabilizing sperm mitochondria in which the autophagosome machinery was impaired. Therefore, this has been suggested as a potential triggering signal for mitophagy in the paternal mitochondria elimination process.

## RESULTS

### Sperm-derived mitochondria are polarized after their entry in the embryo

CMXRos labeling of males to stain sperm mitochondria and track them after fertilization allowed us to observe the fate of these organelles after their entry into the embryo (Al Rawi et al., 2011; Lim et al., 2019; Sato and Sato, 2011; Wang et al., 2016; Zhou et al., 2011, 2016). CMXRos represents a convenient mitochondrial marker but not a good sensor for mitochondrial membrane potential since it binds to internal mitochondrial components. TMRE instead is regarded as a reliable marker of polarized mitochondria since it stains only mitochondria with a membrane potential (Zorova et al., 2018). Intriguingly, experiments crossing TMRE labeled males with unlabeled hermaphrodites did not allow the tracking of sperm-derived mitochondria in the embryos even when isolated

[1]Sorbonne Université, CNRS, Institut de Biologie Paris Seine, IBPS, Developmental Biology Laboratory, UMR7622, Paris, France

[2]Sorbonne Université, CNRS, Institut de Biologie Paris Seine, IBPS, IBPS Imaging Facility, FRE3631 Paris, France

[3]Lead contact

*Correspondence: vincent.galy@sorbonne-universite.fr

https://doi.org/10.1016/j.isci.2020.102029

sperm mitochondria could be labeled (Wang et al., 2016; Zhou et al., 2016). This result was interpreted as a rapid loss of membrane potential of sperm mitochondria after their entry into the oocyte's cytoplasm, however, the loss of the dye was never directly documented by live microscopy (Wang et al., 2016; Zhou et al., 2016). Alternatively, we reasoned that the small number of labeled sperm mitochondria entering an unlabeled oocyte combined with a property of TMRE to translocate in and out of the mitochondria, could lead to the dilution of the TMRE brought by sperm mitochondria. To test this hypothesis and avoid this potential dilution effect we provided TMRE to both sperm- and oocyte-derived mitochondria and monitor fertilization cycles in TMRE labeled animals. 3D-multichannel time-lapse recordings of immobilized young hermaphrodites crossed in presence of TMRE to males with HSP-6::GFP green fluorescent mitochondria allowed the tracking of the sperm mitochondria from their entry into the oocyte (Figure 1A and Video S1). No significant TMRE loss was observed in these conditions. This was confirmed on dissected embryos in Meiosis I and II (Figure 1B). While a complete overlap of TMRE and HSP-6::GFP was observed in meiotic embryos (n = 10) a gradual reduction of the fraction of TMRE labeled sperm mitochondria at the 2-cell and 4-cell stage was observed and quantified with 40,5% (n = 14) and 8% (n = 16) respectively (Figure 1C). Furthermore, we measured a 13 s half-recovery time of more than 80% of TMRE fluorescence after photobleaching of sperm-mitochondria (n = 11), consistent with polarized mitochondria and the dynamic exchange of the fluorescent marker in and out of sperm-derived mitochondria (Figure S1). Finally, addition of CCCP (carbonyl cyanide m-chlorophenylhydrazone) on early permeable embryos leads to the complete loss of TMRE from all mitochondria including sperm-derived mitochondria in 100% of the treated embryos but never in DMSO (dimethyl sulfoxide) alone controls (Figure 1D, n = 24 and n = 25, respectively), demonstrating that TMRE labeling of sperm-derived mitochondria was due to their membrane potential. The polarization of sperm-derived mitochondria was confirmed in 100% of meiotic embryos (n = 14) using TMRM (tetramethylrhodamine methyl ester), another cationic fluorescent dye accumulating in polarized mitochondria (Figure S2).

## Autophagy targets polarized globular sperm-derived mitochondria

*C. elegans* sperm mitochondria were shown to have a globular shape in the fertilized embryo (Wang et al., 2016), raising the hypothesis that this morphology may be important for their entry into the autophagy pathway. Interestingly, interference with the maternal mitochondria dynamics had a modest impact on the kinetic of sperm-derived mitochondria clearance (Wang et al., 2016). The fragmentation of maternal mitochondria in a fusion mutant was suggested to distract the autophagy machinery from the sperm-derived mitochondria (Wang et al., 2016). Our morphological analysis by non-invasive gentle imaging of TMRE labeled mitochondria at the time of autophagosome formation around the sperm mitochondria (*i.e.* anaphase of meiosis I) revealed that the maternal mitochondria are fragmented in globular and rod shape mitochondria and acquire their tubular shape only later, during the first mitotic division. Indeed, TMRE labeling of all mitochondria showed that maternal mitochondria are organized as long tubes from the first mitosis (Figure 2A) to later stages (Figure 4 and Video S2). The differential morphology of the sperm-versus oocyte-derived mitochondria is therefore not likely critical for their specific targeting of sperm mitochondria.

The observation that sperm mitochondria remain polarized at the one cell stage (Figure 1B) suggested that the formation of the autophagosomes would occur around polarized sperm mitochondria. Indeed, as anticipated, based on the TMRE labeling of all sperm mitochondria at the end of the second meiotic division (Figure 1B) plus the known timing of allophagosomes formation (Al Rawi et al., 2011; Djeddi et al., 2015; Sato and Sato, 2011), we observed that, in living embryos, LGG-1::GFP recruitment occurred around TMRE labeled sperm mitochondria at the end of the first female meiotic division and during the second meiotic division (Figure 2B). We have previously demonstrated that there is a complete overlap of TMRE signal and sperm mitochondria until the end of meiosis II (Figure 1B). Therefore, we can safely assume that all sperm mitochondria are TMRE positive at this point. This showed that the loss of membrane potential of sperm-inherited mitochondria is not an early step in autophagosomes formation and is not required to initiate the process like in other mitophagy pathways (Ding and Yin, 2012).

## Loss of membrane potential of sperm mitochondria requires autophagy

Since the fraction of sperm mitochondria labeled with TMRE strongly decreases between the 2- and 4-cell stage after their entry in autophagosomes, we wondered whether the loss of membrane potential requires their entry in the autophagy pathway. Thus, we tested if the mitochondrial membrane potential of sperm mitochondria would be maintained when autophagosome formation is impaired and sperm mitochondria remains present in late stage embryos. Sperm mitochondria stabilization is observed when key factors of the allophagy machinery such LGG-1 and ALLO-1 are impaired. ALLO-1 is an autophagy receptor that directly binds to the worm's LC3

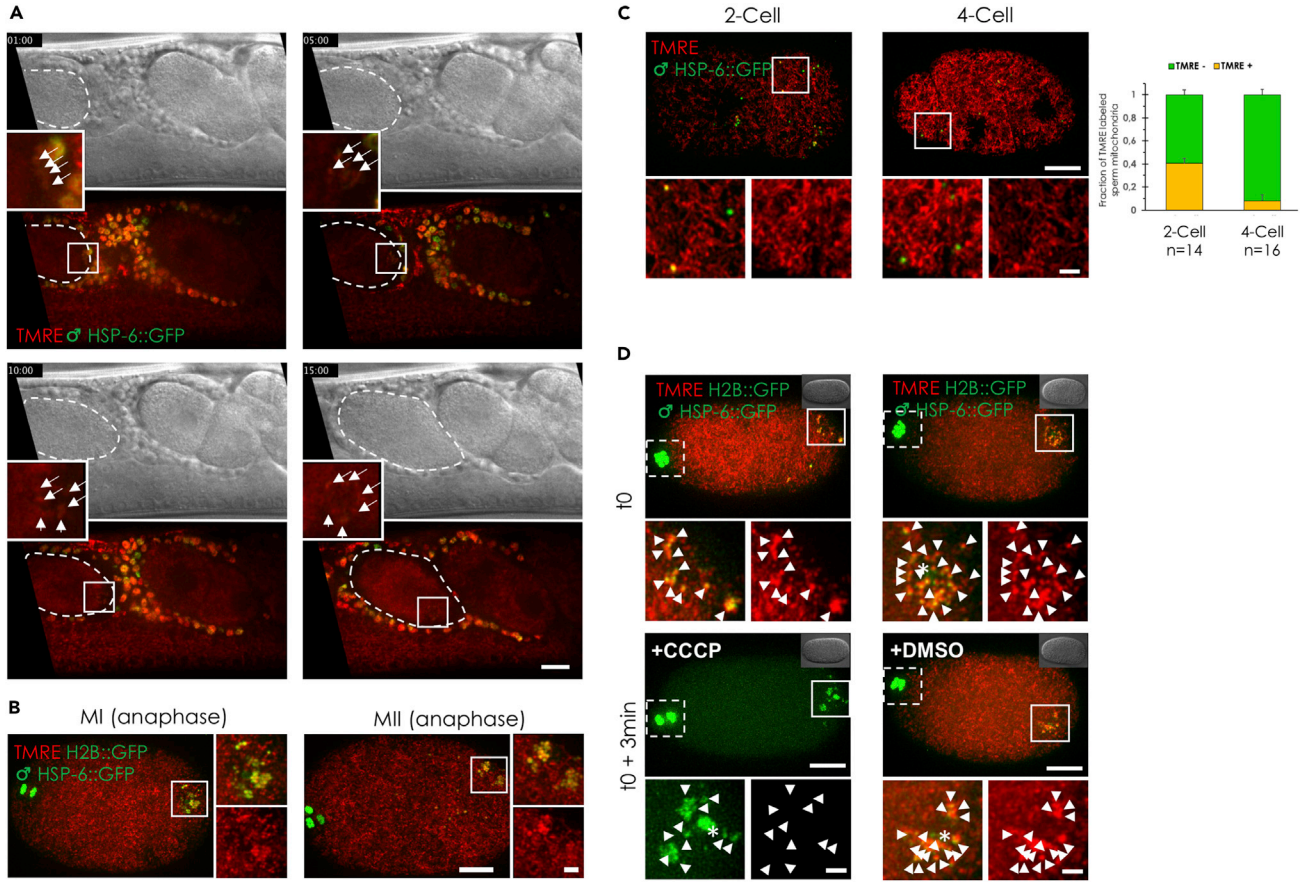


**Figure 1. Sperm mitochondria remain polarized after fertilization**

Males expressing mitochondrial marker HSP-6::GFP in the germline were crossed on TMRE plates overnight with N2 (A and C) or histone H2B::GFP expressing hermaphrodites to follow the transition from oocyte nuclear breakdown to meiotic divisions (B and D). Maternal and sperm derived mitochondria are labeled with TMRE (red) and sperm-derived mitochondria are tracked with the HSP-6::GFP marker (green). Chromatin is also marked with histone H2B::GFP (green) to identify the embryonic stage (B and D), unless otherwise stated.

(A) Still images of time-lapse of *in-utero* fluorescence spinning disk and DIC imaging of the fertilization process. Crossed hermaphrodites were immobilized with 15 μm beads and 30 μM tetramizole on 2% agar pads before imaging. Maximum intensity Z-projections of 5 selected plans containing the tracked sperm mitochondria (arrow) through the process of fertilization (t = 0 min) and every 5 min. During the 15 min covered by these still images, sperm mitochondria remain labeled with TMRE in the newly fertilized oocyte (dash line). Scale bar: 10 μm.

(B) Hermaphrodites were dissected in meiosis buffer with 15 μm beads and early embryos were carefully released and mounted for imaging between a slide and a coverslip. Maximum intensity Z-projections of 25 consecutives deconvolved spinning disk images (400 nm apart) of Meiosis I (MI) (left panel) and II (MII) (right panel) of dissected embryos showed TMRE labeled sperm mitochondria. Magnified views of merged TMRE and HSP-6::GFP or TMRE channels highlighted areas are shown next to each panel. Note TMRE-labeled sperm mitochondria. Scale bars: 10 μm and 2 μm (overviews and insets, respectively).

(C) Sperm-derived mitochondria gradually lose TMRE fluorescence during early zygotic cell divisions. Maximum intensity Z-projections of 16 consecutives deconvolved spinning disk images (400 nm apart) of 2 and 4 cells stage dissected embryos (left panels). Magnified views of merged TMRE and HSP-6::GFP or TMRE channels highlighted areas are shown next to each panel. Percentage of TMRE-labeled sperm derived mitochondria in 2 and 4 cells embryos (n = 14 and n = 16, respectively) are significantly different (unpaired t test, p value <0.0001). Scale bars: 10 μm and 2 μm (overviews and insets, respectively) and error bars represent s.e.m.

(D) TMRE labeling of sperm-derived mitochondria reflects their membrane potential. Maximum intensity Z-projections of 23 consecutives deconvolved spinning disk images (250 nm apart) of MI TMRE labeled embryos prior (t = 0) (top) and 3 min after (bottom) treatment with CCCP (n = 24, left) or DMSO (n = 25, right). Magnified views of merged TMRE and HSP-6::GFP or TMRE channels highlighted areas are shown below each panel. TMRE fluorescence is lost upon CCCP treatment. The maternal meiotic DNA (H2B::GFP) allows to establish embryonic stage (dashed-line box). Arrowheads and asterisk indicate sperm-derived mitochondria and DNA, respectively. Scale bars: 10 μm and 2 μm (overviews and insets, respectively).

homolog LGG-1 through its LC3-interacting region motif (Sato et al., 2018). Homozygote *allo-1(tm4756)* mutant worms are viable and show stabilized sperm-derived mitochondria until late embryonic stage and even in L1 stage worms (Sato et al., 2018). Since homozygote *lgg-1* loss-of-function is lethal, we performed *lgg-1(RNAi)* to stabilized sperm mitochondria in the progeny of heterozygous mutants as previously described (Djeddi et al., 2015). To assess the membrane potential of stabilized sperm-derived mitochondria in late stage embryos,

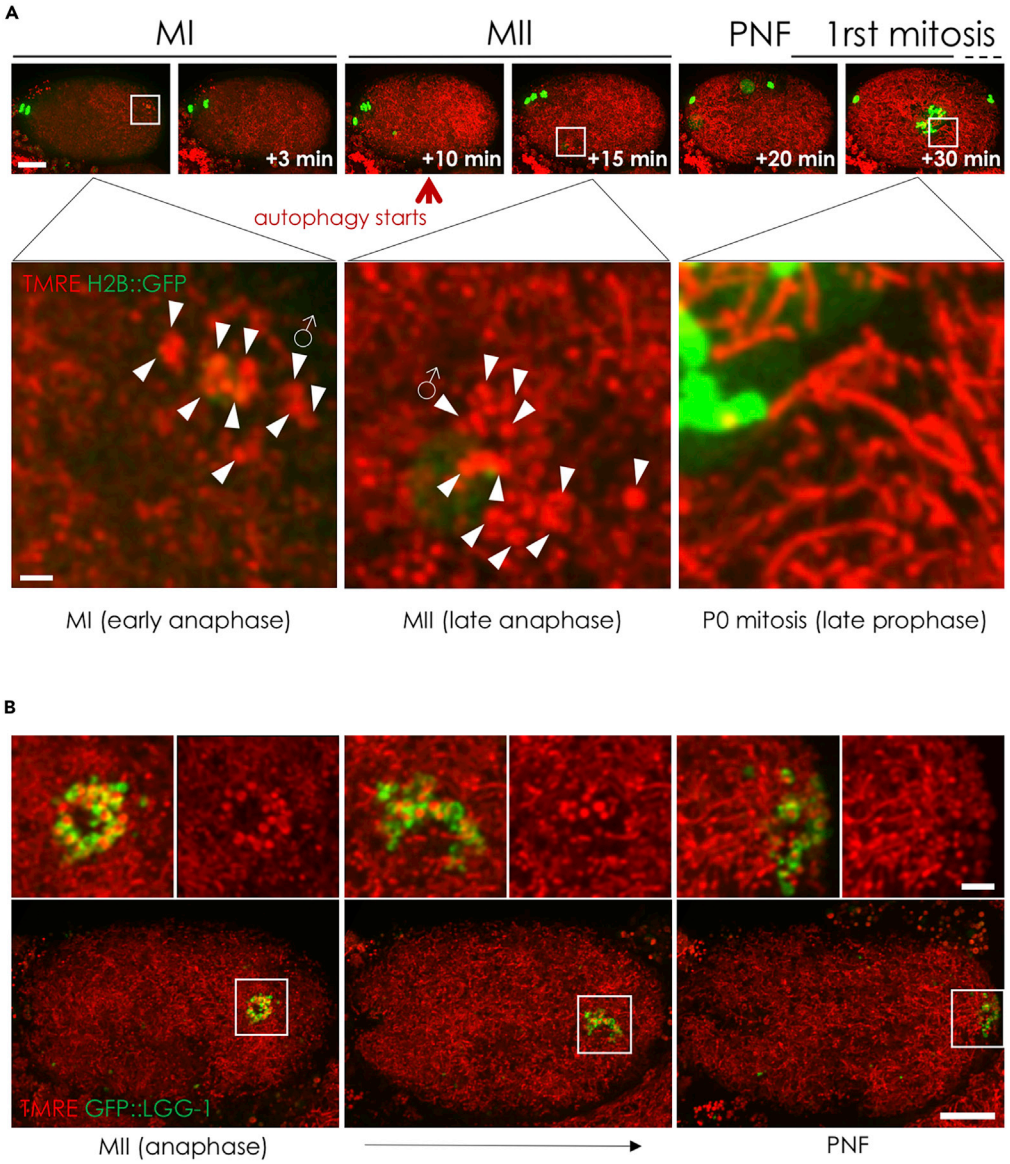


**Figure 2. The autophagy machinery targets polarized and globular sperm mitochondria at the end of the female first meiotic division**

During the first 30 min of embryonic development, Meiosis I (MI) and II (MII), pronuclear formation (PNF) and the first mitosis take place. Recruitment of autophagy machinery starts during late MI. Oocyte and sperm-derived mitochondria are labeled with TMRE (red) in all panels.

(A) Maternal mitochondria change their shape and organization during the first hour after fertilization. Maximum intensity Z-projections of 21 consecutives deconvolved spinning disk images (400 nm apart) of TMRE-labeled embryos expressing Histone H2B::GFP (green). Sperm mitochondria (arrowhead) show unique spherical shape while oocyte-derived mitochondria change from fragmented and rod shape (MI) and become tubular (prometaphase of the first mitosis). Scale bar: 10 μm (top) and 1 μm (bottom).

(B) Autophagy marker LGG-1 is recruited around polarized sperm mitochondria. Maximum intensity Z-projections of 61 deconvolved spinning disk images (250 nm apart) of TMRE-labeled embryos expressing LGG-1::GFP (green). TMRE-labeled sperm mitochondria are surrounded by LGG-1 forming the autophagosome while the $\Delta\Psi m$ is maintained until the PNF stage. Scale bars: 2 μm (top) and 10 μm (bottom).

we crossed LGG-1 depleted or *allo-1(tm4756)* mutant hermaphrodites with HSP-6::GFP males in the presence of TMRE. Using GFP as a marker we observed that only a small fraction of the total sperm mitochondria lost the TMRE signal and we quantified that 88% and 84% of the total sperm mitochondria remains polarized in *lgg-1*

and *allo-1* depleted 24-cell embryos, respectively (Figure 3A). Additionally, after CCCP treatment, 100% of *allo-1(tm4756)* permeabilized (*perm-1(RNAi)*) TMRE labeled late embryos completely lost TMRE in all mitochondria including sperm-derived mitochondria (Figure 3B, n = 33) while no loss was observed in DMSO-treated control embryos (Figure 3B, n = 31). All together our results demonstrate that TMRE labeling of sperm-derived mitochondria was due to their membrane potential.

### Stabilized sperm-derived mitochondria remain polarized and distinct from oocyte-derived mitochondria

While studying the membrane potential of stabilized sperm mitochondria, we noticed that these mitochondria looked to be in close proximity and closely associated with maternal mitochondria. Using live time-lapse recordings of TMRE-labeled *allo-1(tm4756)* embryos with the GFP sperm mitochondria marker (HSP-6::GFP), we observed that sperm mitochondria remained as individualized spherical structures laying in closed contact with the tubular shaped maternal mitochondria (Figure 4A) at all times (Video S3). HSP-6 is a mitochondrial matrix protein. Interestingly, our observation suggested that there is no transfer of HSP-6::GFP protein from the sperm to the maternal mitochondria. To further test the ability or not of sperm mitochondria to fuse with the maternal mitochondria, we tested if we could observe some protein exchange between both sperm and maternal mitochondrial outer membranes. Thus, we used two reporter strains for mitochondria outer membrane (MOM) proteins. For the maternal outer membrane, we used CRISPR-Cas9 fusion (Paix et al., 2017) between *gfp* and *tomm-20* to generate a reporter strain. Tom20/TOMM-20 is part of the translocase of the outer membrane complex (TOM complex) and is a receptor protein encoded in the nucleus (Becker et al., 2009; Neupert and Herrmann, 2007). As expected the TOMM-20::GFP fusion protein was broadly expressed in somatic tissues as well as in the germline oocytes and sperm. To be able to study stabilized sperm mitochondria, this fusion protein was introduced into the *allo-1(tm4756)* mutant strain. The fusion protein mRuby3::FNDC-1 was used as an MOM marker in sperm mitochondria. FUNDC1 (FUN14 domain containing 1), FNDC-1 homolog in *C. elegans*, is an MOM protein involved in the clearance of mitochondria damaged by exposure to hypoxia and has being recently involved in paternal mitochondria elimination (Lim et al., 2019; Liu et al., 2012). Interestingly, we did not observe any exchange of MOM proteins between the maternal and paternal mitochondria in late embryos (Figure 4B).

## DISCUSSION

Transmission electron microscopy analysis in the 1-cell stage *C. elegans* embryo revealed that sperm mitochondria can be distinguished from the maternal ones as they have circular sections, while the oocyte-derived mitochondria show sections of elongated shapes ((Zhou et al., 2016), our unpublished results). Furthermore, the average diameter of the wild-type sperm mitochondria is around 460 nm while for the more tubular maternal ones the average short diameter is around 240 nm (Zhou et al., 2016). Here, we used live imaging of mitotracker labeled embryos and revealed that the oocyte-derived mitochondria are fragmented during meiotic division and the tubular shape is evident only from the first mitotic division. Despite this modest morphological difference between sperm- and oocyte-derived mitochondria in the first minutes after fertilization, the embryo specifically recognizes and targets the sperm-derived population. Therefore, this result suggests that the fragmented property of the sperm mitochondria is not likely a major criterion for the specificity of their autophagy targeting. Another suspected triggering property of the sperm mitochondria was the loss of their membrane potential after their entry into the ooplasm. Rosamine-based MitoTracker dyes like CMXRos are sequestrated inside the mitochondria where they bind to intramitochondrial components allowing us to track mitochondria in fixed samples; however, this makes them poor reporters of changing mitochondrial membrane potential ($\Delta\Psi m$)(Zorova et al., 2018). In contrast, the lipophilic cationic dye TMRE accumulates in the mitochondrial matrix proportionally to the magnitude of the membrane potential electronegativity (Ehrenberg et al., 1988) which makes it a suitable tool to estimate mitochondrial membrane potential. Importantly, TMRE is not retained in fixed samples and its distribution is highly sensitive to the experimental conditions and therefore it must be used carefully and in proper experimental conditions. The *C. elegans* embryo is fragile and prone to irreversible damage during the first minutes of development, especially prior egg-shell formation. Thus, the absence of TMRE signal previously reported (Sato et al., 2018; Wang et al., 2016; Zhou et al., 2016) could have been caused by the observation of damaged embryos due to osmotic change, photo toxicity or even physical damage. We showed that sperm-derived mitochondria are TMRE and TMRM positive and only lose their membrane potential once inside the autophagosomes. We also tested the ability of TMRE to go in-and-out of sperm mitochondria within the embryo. Using FRAP (fluorescence recovery after photobleaching) in TMRE labeled embryos, we observed that once a single sperm mitochondrion was targeted and photobleached, fluorescence was recovered within less than a minute (Figure S1). This observation indicates that (i) uptake of new TMRE by sperm mitochondria is possible suggesting a

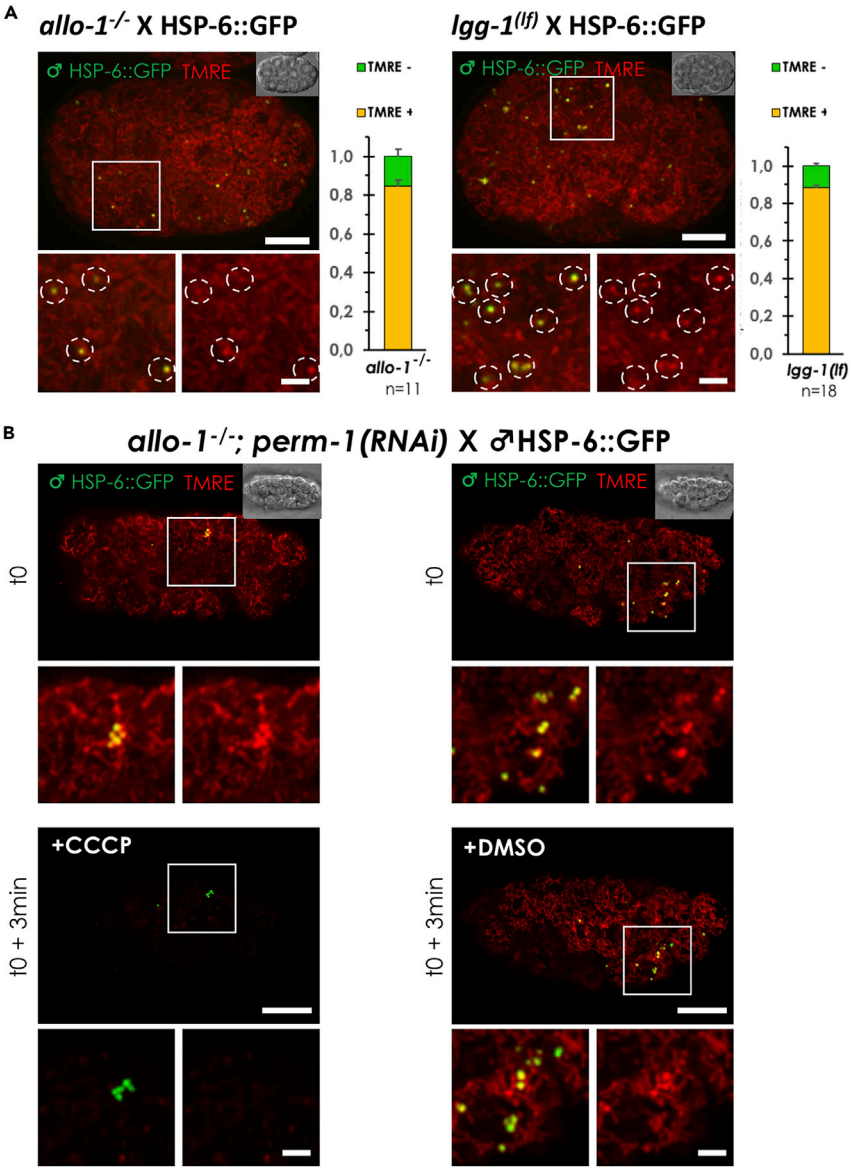


**Figure 3. Loss of membrane potential of sperm mitochondria requires autophagy**

Sperm mitochondria were stabilized in *allo-1* or *lgg-1* loss-of-function. Males expressing the mitochondrial HSP-6::GFP marker in the germline were crossed with *allo-1(tm4756)* and *lgg-1(tm3489); lgg-1(RNAi) (lgg-1(lf))* mutants hermaphrodites. Oocyte and sperm mitochondria were labeled with TMRE (red) and sperm-derived mitochondria tracked with the HSP-6::GFP marker (green).

(A) Maximum intensity Z-projections of spinning disk images of 20-24 cell embryos. Two-fold magnification of a single plane of the highlighted areas are shown below each panel. Sperm mitochondria GFP signal co-localizes with TMRE fluorescence in *allo-1(tm4756)* and *lgg-1(lf)* (in circles). Fraction of TMRE-labeled sperm mitochondria is 0.84 (n = 11) and 0.88 (n = 18), respectively. Scale bars: 10 μm (top) and 2 μm (bottom). Error bars represent the s.e.m. In both cases the fraction of TMRE labeled and non-labeled sperm mitochondria are significantly different (paired t test – p *value* > 0.0001).

(B) Maximum intensity Z-projections of spinning disk images of 20-24-cell stage *allo-1(tm4756)*, *perm-1(RNAi)* embryos before (t = 0) and after treatment by CCCP or DMSO alone (t = 0 +3min). *perm-1(RNAi)* treatment is used for the permeabilization of the embryo's eggshell to permit CCCP incorporation. Two-fold magnification of a single plane of the highlighted areas are shown below each panel, sperm mitochondria GFP signal co-localizes with TMRE fluorescence prior treatment. TMRE signal is lost upon CCCP treatment but not affected by DMSO treatment. Scale bars: 10 μm (top) and 2 μm (bottom) and error bars represent the s.e.m.

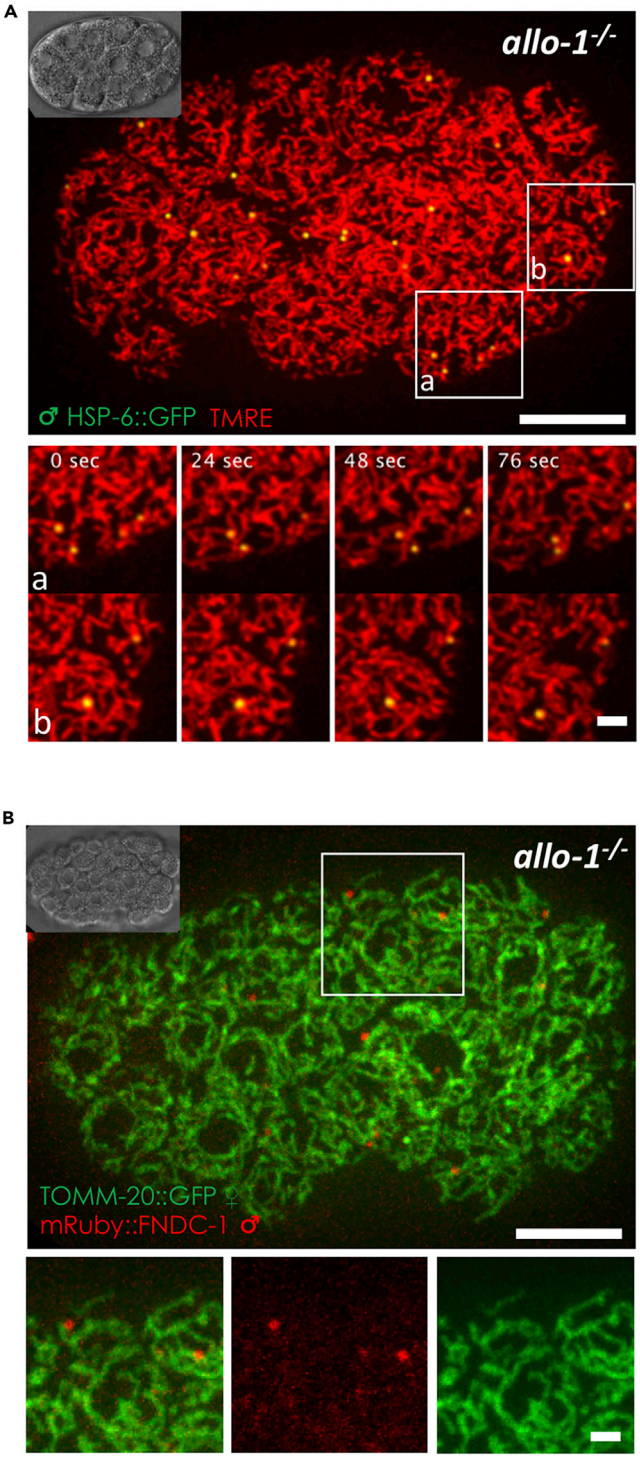


**Figure 4. Stabilized sperm mitochondria are associated with maternal mitochondria**

Sperm mitochondria are stabilized in *allo-1*(tm4756) mutant worms and move along with maternal mitochondria in the embryos, without exchange of mitochondrial outer membrane (MOM) proteins between them.

(A) *allo-1(tm4756)* hermaphrodites were crossed with HSP-6::GFP males in the presence of TMRE. Maternal and paternal mitochondria are both labeled with TMRE in the embryo (red) where sperm-derived mitochondria can be tracked with the HSP-6GFP marker (green). Maximum intensity Z-projections of 13 spinning disk deconvolved live images of a 24-cell stage

**Figure 4. *Continued***
embryo. z stack images were acquired every 0.24 μm on a spinning disk microscope every 4 s. Magnifications of 2 highlighted areas are shown below. Scale bars: 10 μm (top) and 2 μm (bottom).
(B) *allo-1(tm4756)*; *tomm-20::GFP* young adult hermaphrodites were crossed with *mRuby::fndc-1* males. Maximum intensity Z-projections of 7 spinning disk live images of a 60-cell stage embryo. Maternal MOM TOMM-20::GFP protein (green) and sperm MOM mRuby::FNDC-1protein (red) are both still visible and do not overlap suggesting that there is no exchange between the membranes of the two types of mitochondria. Magnifications of the merge and individual channels of the highlighted area are shown below. Scale bars: 10 μm (top) and 2 μm (bottom).

dynamic exchange of the dye within the embryo, and (ii) sperm mitochondria membrane potential is not lost before autophagosome formation.

Additionally, the loss of function of the autophagy factors, such as ALLO-1 and LGG-1, revealed that stabilized sperm-derived-mitochondria can maintain their membrane potential even in late embryonic stages in the absence of the autophagy machinery. Our results suggest that loss of membrane potential requires the entry of the mitochondria into the autophagosome, eliminating the possibility of it being the triggering signal for autophagy factors recruitment.

Intriguingly, in later embryonic stages, sperm mitochondria remain in spherical shape, and even when they seem to be closely associated with the surrounding maternal mitochondria, we did not observe them fused with the maternal mitochondria nor any exchange of mitochondrial proteins between sperm and maternal mitochondria.

It is becoming clearer that sperm mitochondria have function during early steps of embryonic development (De Henau et al., 2020), but after this role is fulfilled, a delicate and precise process of elimination by autophagy is carried out to insure a strict maternal inheritance. Our results suggest that if this process fails, a backup system that prevents sperm mitochondria integration into the mitochondrial network could be acting as a last resort.

More work is required to identify the triggering and selective mechanism for sperm mitochondria removal and the additional mechanism(s) preventing sperm mitochondrial DNA leakage.

## Limitations of the study

The fact that sperm mitochondria remain polarized and separated from the maternal mitochondrial network until their entry into the autophagosomes in the *C. elegans* embryo argues for a late loss of integrity of the mitochondria and a mechanism preventing their fusion. All the known mechanisms involved in the clearance of sperm-mitochondrial DNA are also at work in *C. elegans* but our discoveries may highlight a remarkable stability (like for the late involvement of the endonuclease G only after fertilization) and suggests that *C. elegans* sperm-mitochondria clearance may happen later in this organism compared to other organisms including vertebrates.

These two properties may also exist in mammalian embryos but are technically challenging to address and beyond the scope of this work. The complete process of sperm mitochondria clearance takes several days in mammals compared to few hours in the *C. elegans* embryo, and mitochondria are particularly sensitive to experimental conditions.

## Resource availability

### *Lead contact*

Further request and information for resources and reagents used in this published article should be directed and will be fulfilled by the lead contact, Vincent Galy, vincent.galy@sorbonne-universite.fr.

### *Materials availability*

All data analyzed and generated in this research are included in this published article and Supplemental information.

### *Data and code availability*

The published article includes all data generated in this study.

## METHODS

All methods can be found in the accompanying Transparent methods supplemental file.

## SUPPLEMENTAL INFORMATION

Supplemental information can be found online at https://doi.org/10.1016/j.isci.2020.102029.

## ACKNOWLEDGMENTS

We are very grateful to Dr M. Labouesse for giving us access to his FRAP microscope, to V. Peletier, V. Parrales, and R. Zamy for valuable technical assistance during all stages of this project. Some strains were provided by the Caenorhabditis Genetic Center, which is funded by NIH Office of Research Infrastructure Programs, USA (P40 OD010440). This work was supported by the Bettencourt Schueller Foundation, France (Coups d'élans pour la recherche to V.G.); the Agence Nationale de la Recherche, France (ANR 12-BSV2-0018-01 to V.G.); the Fondation pour la Recherche Médicale, France (Equipe FRM DEQ20160334874 to V.G. and K.R.) and by the ARC Foundation, France (fellowship to S.A.).

## AUTHOR CONTRIBUTIONS

K.R., S.A., F.H., and J.M. conducted the experiments; F.L. deconvolved the images; K.R. and V.G. designed and analyzed the experiments and wrote the paper.

## DECLARATION OF INTERESTS

The authors declare no competing interests.

Received: September 16, 2020
Revised: December 17, 2020
Accepted: December 29, 2020
Published: January 22, 2021

## REFERENCES

Al Rawi, S., Louvet-Vallee, S., Djeddi, A., Sachse, M., Culetto, E., Hajjar, C., Boyd, L., Legouis, R., and Galy, V. (2011). Postfertilization autophagy of sperm organelles prevents paternal mitochondrial DNA transmission. Science *334*, 1144–1147.

Becker, T., Gebert, M., Pfanner, N., and van der Laan, M. (2009). Biogenesis of mitochondrial membrane proteins. Curr. Opin. Cell Biol. *21*, 484–493.

De Henau, S., Pagès-Gallego, M., Pannekoek, W.J., and Dansen, T.B. (2020). Mitochondria-derived H2O2 promotes symmetry breaking of the *C. elegans* zygote. Dev. Cell *53*, 263–271.

DeLuca, S.Z., and O'Farrell, P.H. (2012). Barriers to male transmission of mitochondrial DNA in sperm development. Dev. Cell *22*, 660–668.

Ding, W.X., and Yin, X.M. (2012). Mitophagy: mechanisms, pathophysiological roles, and analysis. Biol. Chem. *393*, 547–564.

Djeddi, A., Al Rawi, S., Deuve, J.L., Perrois, C., Liu, Y.Y., Russeau, M., Sachse, M., and Galy, V. (2015). Sperm-inherited organelle clearance in *C. elegans* relies on LC3-dependent autophagosome targeting to the pericentrosomal area. Development *142*, 1705–1716.

Ehrenberg, B., Montana, V., Wei, M.D., Wuskell, J.P., and Loew, L.M. (1988). Membrane potential can be determined in individual cells from the nernstian distribution of cationic dyes. Biophys. J. *53*, 785–794.

Lim, Y., Rubio-Peña, K., Sobraske, P.J., Molina, P.A., Brookes, P.S., Galy, V., and Nehrke, K. (2019). Fndc-1 contributes to paternal mitochondria elimination in *C. elegans*. Dev. Biol. *454*, 15–20.

Liu, L., Feng, D., Chen, G., Chen, M., Zheng, Q., Song, P., Ma, Q., Zhu, C., Wang, R., Qi, et al.. (2012). Mitochondrial outer-membrane protein FUNDC1 mediates hypoxia-induced mitophagy in mammalian cells. Nat. Cell Biol. *14*, 177–185.

Neupert, W., and Herrmann, J.M. (2007). Translocation of proteins into mitochondria. Annu. Rev. Biochem. *76*, 723–749.

Paix, A., Folkmann, A., and Seydoux, G. (2017). Precision genome editing using CRISPR-Cas9 and linear repair templates in *C. elegans*. Methods *121–122*, 86–93.

Politi, Y., Gal, L., Kalifa, Y., Ravid, L., Elazar, Z., and Arama, E. (2014). Paternal mitochondrial destruction after fertilization is mediated by a common endocytic and autophagic pathway in Drosophila. Dev. Cell *29*, 305–320.

Sato, M., and Sato, K. (2011). Degradation of paternal mitochondria by fertilization-triggered autophagy in *C. elegans* embryos. Science *334*, 1141–1144.

Sato, M., Sato, K., Tomura, K., Kosako, H., and Sato, K. (2018). The autophagy receptor ALLO-1 and the IKKE-1 kinase control clearance of paternal mitochondria in *Caenorhabditis elegans*. Nat. Cell Biol. *20*, 81–91.

Song, W.-H., Yi, Y.-J., Sutovsky, M., Meyers, S., and Sutovsky, P. (2016a). Autophagy and ubiquitin–proteasome system contribute to sperm mitophagy after mammalian fertilization. Proc. Natl. Acad. Sci. U S A *113*, E5261–E5270.

Song, W.H., Yi, Y.J., Sutovsky, M., Meyers, S., and Sutovsky, P. (2016b). The ART and science of sperm mitophagy. Autophagy *12*, 2510–2511.

Sutovsky, P., and Song, W.H. (2018). Post-fertilisation sperm mitophagy: the tale of mitochondrial Eve and Steve. Reprod. Fertil. Dev. *30*, 56–63.

Wang, Y., Zhang, Y., Chen, L., Liang, Q., Yin, X.M., Miao, L., Kang, B.H., and Xue, Di. (2016). Kinetics and specificity of paternal mitochondrial elimination in *Caenorhabditis elegans*. Nat. Commun. *7*, 12569.

Zhou, Q., Li, H., Li, H., Nakagawa, A., Lin, J.L.J., Lee, E.-S., Harry, B.L., Skeen-Gaar, R.R., Suehiro, Y., William, et al.. (2016). Mitochondrial endonuclease G mediates breakdown of paternal mitochondria upon fertilization. Science *353*, 394–399.

Zhou, Q., Li, H., and Xue, D. (2011). Elimination of paternal mitochondria through the lysosomal degradation pathway in *C. elegans*. Cell Res *21*, 1662–1669.

Zorova, L.D., Popkov, V.A., Plotnikov, E.Y., Silachev, D.N., Pevzner, I.B., Jankauskas, S.S., Babenko, V.A., Zorov, S.D., Balakireva, A.V., Juhaszova, et al.. (2018). Mitochondrial membrane potential. Anal. Biochem. *552*, 50–59.

**iScience, Volume *24***

## Supplemental Information

# Mitophagy of polarized sperm-derived mitochondria after fertilization

**Karinna Rubio-Peña, Sara Al Rawi, Fanny Husson, France Lam, Jorge Merlet, and Vincent Galy**

**Supplemental Information**

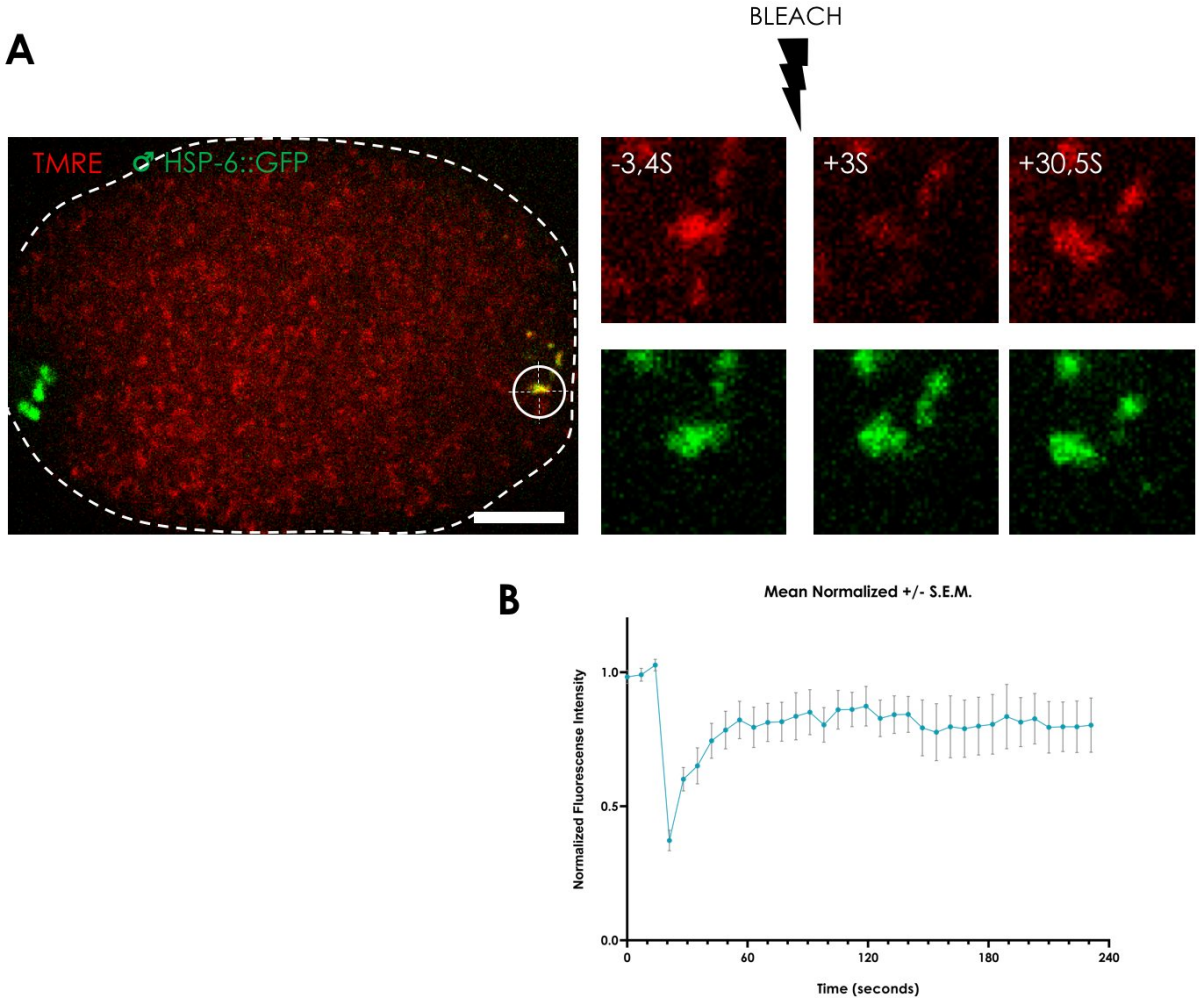


**Figure S1. TMRE labeled sperm-derived mitochondria is able to recover fluorescence after photobleaching in early embryos, *Related to figure 1.***

Fluorescence recovery after photobleaching (FRAP) is analyzed in TMRE labeled embryos within 20 minutes after fertilization. (A) Sperm mitochondria (HSP-6::GFP, green) is targeted with 100 % intensity laser (7-10 px) and fluorescence recovery is recorded. Single stack images of the targeted sperm mitochondria over time are shown (right panels). (B) Normalized fluorescence intensity data over time is displayed in the graph. Error bars represent s.e.m. n= 11. Scale bar: 10 μm.

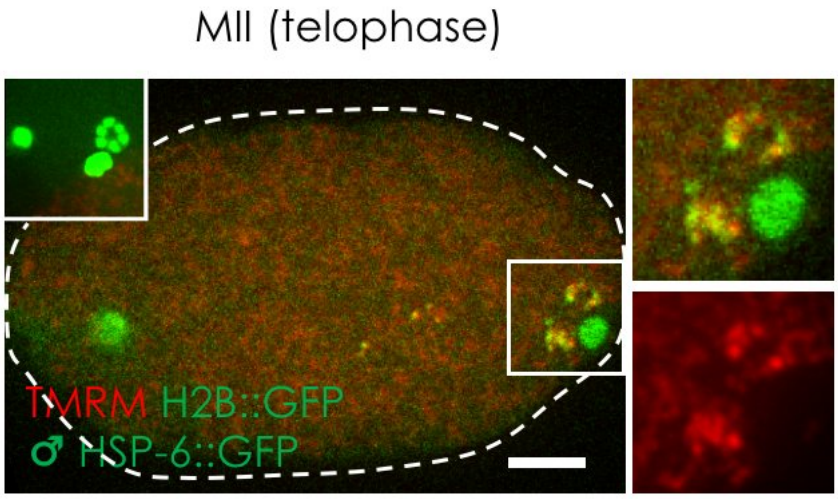


***Figure 2S. Sperm-derived mitochondria are labelled with TMRM in early embryos, Related to figure 1B***

Males expressing the HSP-6::GFP mitochondrial marker in the germline were crossed with Histone H2B::GFP expressing hermaphrodites in the germline on 2.5 µM TMRM plates. Maternal and sperm-derived mitochondria are labeled with TMRM (red) and sperm-derived mitochondria are highlighted with the HSP-6::GFP marker (green). Chromatin is also marked with histone H2B::GFP (green) to identify the embryonic stage. TMRM labeling of sperm-derived mitochondria reflects their membrane potential. A single plane of spinning disk images of a late MII (telophase) embryos is presented (n= 14). A maximum intensity Z-projection of the histone GFP maternal chromatin reveal the stage of meiosis (left inset). Magnified views of merged TMRM, histone H2B::GFP and HSP-6::GFP or TMRM channels highlighted areas are shown on the right. Scale bar: 10 µm

**Transparent Methods**

***C. elegans* strains and maintenance**

Strains were maintained under standard conditions at 15 or 20 °C on *E. coli* OP50 seeded NGM plates. For knockdown experiments, bacterial clones from the J. Ahringer library (Kamath and Ahringer, 2003) (*perm-1*, *lgg-1* and empty vector L4440 for control) were used as previously described (Al Rawi et al., 2011). For *lgg-1* knock-down *lgg-1(tm3489)* L4 worms were fed with *lgg-1* clone for 3 days at 15 °C, crosses were made overnight also at 15 °C. For embryo permeabilization using *perm-1* knock-down (Carvalho et al., 2011), *allo-1(tm4756)* L4 worms were feed with *perm-1* (RNAi) bacterial clone for 2.5 days at 15 °C and then crossed with *HSP-6::GFP* males overnight at 20 °C on fresh NGM plates seeded with the *perm-1 (*RNAi) clone. Strains used in this study were the parental N2 Bristol strain and the following:

| | |
|---|---|
| •*lgg-1(tm3489)* (Djeddi et al., 2015) | *lgg-1(tm3489)/dpy-10(e128);unc-4(e120)* |
| •*allo-1(tm4756)* | *allo-1(tm4756)* back crossed four times |
| •VIG21 (Djeddi et al., 2015) | *pmcls4[Pmex-5::HSP-6::GFP, unc-119(+)] II; unc-119(ed3) III* |
| •VIG56 | *pmcls4[Pmex-5::HSP-6::GFP, unc-119(+)] II unc-119(ed3) III; him-5(1490) V* |
| •AZ212 H2B::GFP (Praitis et al., 2001) | *unc-119(ed3); ruIs32[unc-119(+), pie-1::GFP::H2B] III* |
| •VIG55 | *allo-1(tm4756) IV; tomm-20(pmc7[tomm-20::linker::GFP])V* |
| •KWN722 (Lim et al., 2019) | *fndc-1(rny15 [mRuby3::fndc-1])II; him-5(e1490)V* |

**CCCP treatment**

For loss-of-membrane potential induction, a dilution of Carbonyl cyanide 3-chlorophenylhydrazone (Sigma-Aldrich, C2759) in 0.9X Meiosis buffer medium (60 % Leibovitz's L-15 Medium no phenol red, 20 % FBS, 0.5 mg/ml Inulin, 25 mM HEPES) was applied directly on the embryos. After 3 minutes, a post CCCP image was taken. Final concentrations for CCCP were 10 µM for *perm-1(RNAi)* embryos and 50 µM for early embryos before eggshell formation. DMSO dilution (1/100 in 0.9X Meiosis buffer) was used as a control.

**TMRE and TMRM staining**

To stain embryos mitochondria, young adult hermaphrodites were grown for 12-16 hours in the dark on NGM plates containing TMRE (2.5 µM) or TMRM (2.5 µM) and seeded with OP50 bacteria. For the staining of embryos from a cross, males and hermaphrodites mating were done overnight at 15 °C on TMRE or TMRM containing plates.

For CCCP treatment of permeable embryos, TMRE was added directly on to the dissected embryos (33 nM in 0.9X Meiosis Buffer).

**Quantification of TMRE positive sperm mitochondria**

HSP-6::GFP males were crossed with wildtype, *allo-1(tm4756)* or *lgg-1(tm3489); lgg-1(RNAi) (lgg-1(lf))* young adult hermaphrodites. Gravid hermaphrodites were dissected on a slide in Meiosis buffer with calibrated 15µm polystyrene beads (Polyscience, 64155-15), covered with a coverslip and sealed with Va-La-P (Vaselin-Lanolin-Parafin, 1:1:1) (Askjaer et al., 2014). Mounted samples are imaged as Z-stacks on a Zeiss Cell Observer spinning disk microscope. For all experiments, numbers HSP-6::GFP labeled mitochondria co-labelled with TMRE were counted from the first 16 Z-images corresponding to the first micrometers of the embryos' volume facing the coverslip.

**Live imaging**

Fluorescence and DIC images were acquired simultaneously or sequentially on a Zeiss Cell Observer spinning disk microscope equipped with a Yokogawa CSU-X1 spinning disk head, 2 Evolve EM CCD cameras and a 1.46 NA 100X objective as single images (for DIC) or multichannel stacks (for fluorescence) of images every 1.5 µm (in utero), 0.4 µm or 0.25 µm (dissected embryos). When

maximum intensity Z-projections are presented, they were generated using Fiji (Schlindelin et al., 2012) or Zen 2012 (blue edition) in order to count the number of particles.

**Deconvolution**

Spinning-disk images obtained with 0.25 or 0.4 µm z steps and 100x 1.46 NA objective were deconvoluted with the commercial deconvolution software Huygens. GMLE (Good's Roughness Maximum Likelihood Estimation) algorithm was used to handle high-noise images and the result was optimized by fine-tuning the regularization parameter SNR (Signal to Noise ratio).

**In utero recording**

*hsp-6::gfp, him-5* males (VIG56) were crossed with *Histone H2B::gfp* young adult hermaphrodites for 12-16 hours in the dark on NGM plates containing TMRE (2.5 µM) with fresh overgrown OP50 bacteria layer. 3-4 worms were anesthetized in a drop of tricaine/tetramisol and then transferred in 3.5 µl of 100 nm polystyrene beads suspension (Polyscience, 00876-15), mounted on a 4 % agarose pad in water and sealed using Va-La-P.

**Generation of the *tomm-20::GFP* transgenic worm**

*tomm-20::gfp* knock-in transgenic worm line was generated via CRISPR Cas9-triggered homologous recombination following a co-CRISPR strategy (Kim et al., 2014). Briefly, crRNAs, tracrRNA and Cas9 were obtained from Integrated DNA Technologies, Inc. The ribonucleoprotein complex containing crRNAs, tracrRNA and Cas9 were annealed at 37°C for 15 minutes prior to injection. A crRNA containing a guide sequence with an adjacent protospacer motif (PAM) in the C-terminal region of tomm-20 (ACACCGACGACTTGGAGTAA TGG) was injected with Cas9 enzyme and *dpy-10* crRNA as a co-injection marker. The PCR repair template containing the (Gly)5Ala::gfp (S65C) coding sequence with 35 nucleotids arms homologous to the genome on both side of the cleavage site that disrupted the PAM was obtained from the amplification of plasmid pJA256 (Zeiser et al., 2011) using TCCAAGAGCTTATCGATGACACCGACGACT-TGGAG-GGAGGTGGAGGTGGAGCT and GAAAGTTAATAAAACTTTTAAATCATTATCCATTATT-TGTATA-GTT-CGTCCATGCCA as forward and reverse primers respectively. The transgenic strain was outcrossed to the ancestral N2 strain 4 times (VIG46) and then crossed with *allo-1(tm4657)* strain (VIG55).

**FRAP**

The FRAP experiments were conducted on Zeiss Axio Observer Z1 microscope equipped with a Yokogawa CSU-X1 spinning disk head, a Roper Ilas2 FRAP module, an Evolve EM CCD camera and a 1.4 NA 100X objective. A pre-bleach image was acquired by averaging three consecutive images. Then a sperm mitochondrion was bleached with a 568 nm laser pulse, lasting between 80 and 180 ms at 100% power. The objective lens used produced a laser spot of 7-10px. Dual channel Z-stack of images were then collected every 3 seconds. For pre- and post- photobleaching imaging, the laser power was typically under 7.5 % of the maximum.

**Supplemental References.**

Askjaer, P., Galy, V., Meister, P. (2014). Modern tools to study nuclear pore complexes and nucleocytoplasmic transport in *Caenorhabditis elegans*, Methods in Cell Biology 122:277-310.

Carvalho, A., Olson, S.K., Gutierrez, E., Zhang, K., Noble, L.B., Zanin, E., Desai, A., Groisman, A., Oegema, K. (2011). Acute drug treatment in the early C. elegans embryo. PLoS One 6(9): e24656.

Kamath, R.S., Ahringer, J. (2003). Genome-wide RNAi screening in *Caenorhabditis elegans*. Methods 30(4):313-21.

Kim, H., Ishidate, T., Ghanta, K.S., Seth, M., Conte, D., Shirayama, M., Mello, C.C. (2014). ACo-CRISPR strategy for efficient genome editing in *Caenorhabditis elegans*. Genetics 197, 1069–1080.

Praitis, V., Casey, E., Collar, D., Austin, J. (2001). Creation of low-copy integrated transgenic lines in *Caenorhabditis elegans*. Genetics 157(3):1217-26.
Schindelin J., Arganda-Carreras, I., Frise, E., Kaynig, V., Longair, M., Pietzsch, T., Preibisch, S., Rueden, C., Saalfeld, S., Schmid, B., *et al.* (2012). Fiji: an open-source platform for biological-image analysis. Nat Methods 9(7):676-82.
Zeiser, E., Frøkjær-Jensen, C., Jorgensen, E., Ahringer, J. (2011). MosSCI and gateway compatible plasmid toolkit for constitutive and inducible expression of transgenes in the *C. elegans* germline. PLoS One 6(5):e20082.